Position regulation of an EGR valve using reset control with adaptive feedforward

Francesco Saverio Panni,*Harald Waschl,*
Daniel Alberer,*Luca Zaccarian†

Abstract

We propose a hybrid control system performing set-point regulation of an Exhaust Gas Recirculation (EGR) valve of a Diesel engine. The control technique is based on a First Order Reset Element (FORE) embedded with an adaptive feedforward action whose aim is to provide asymptotic rejection of disturbances acting at the plant input. The feedforward action is adapted by suitable resetting laws occurring whenever the FORE is reset to zero. We first provide a formal analysis of the effectiveness of the adaptive reset system to guarantee asymptotic set-point regulation, and then we illustrate how the adaptive feedforward can be parametrized for improved transient performance. We experimentally illustrate the proposed solution on a Diesel engine testbench which reveals substantial position accuracy improvement during a standard driving cycle, as compared to the production standard solution.

I. Introduction

The increasingly stringent emission levels for passenger cars lead to continuously increased requirements for combustion engines [9]. On the one hand these requirements are addressed by applying improved and/or new electro-mechanical components, *e.g.*, variable valve timing for spark ignition engines or common rail injection for Diesel engines, and on the other hand enhanced control methods need to be employed in order to exploit the potentialities provided by the electro-mechanical layout. In particular, in the past two decades, the applied nonlinear control community has devoted large attention to this problem both in terms of developing state-space nonlinear control oriented models (see, *e.g.*, [6], [13], [18] and references therein), and in terms of developing nonlinear control solutions mostly exploiting tools from Lyapunov stability theory (see, e.g., [18], [8], [19], [14], [17], [16] the survey paper [4] and references therein). The field of engine control systems is much broader and populated by results which go beyond the narrow field of Lyapunov-based nonlinear control solutions (see for example the well known monograph [6]), but Lyapunov theory is the main tool used in the experimental work presented in this paper.

In recent years, there has been a renewed interest in reset control systems initiated by the early work of Clegg [3]. In particular, the First Order Reset Element (FORE) proposed in [7] has been revisited in [1], [2] and references therein) and has been shown to overcome certain limitations of linear control systems. More recently, using the hybrid systems framework proposed in [5] and references therein, reset control systems have been analyzed by establishing $\mathcal{L}_2$ stability and exponential stability properties also in cases where the underlying linear system is exponentially unstable [10]. This peculiar feature allows to design controllers inducing closed-loop responses consisting in exponentially diverging branches of trajectories which are stabilized by the resetting action of the FORE. Due to this fact, the expected performance is that of a very aggressive (essentially unstable) control action and promises increased effectiveness at rejecting disturbances.

In this work, we employ the set-point regulation scheme proposed in [10] for the position control of an exhaust gas recirculation (*EGR*) valve of a passenger car Diesel engine. Since the scheme of [10] requires knowledge of possible disturbances acting on the plant and also of the plant DC gain, we propose an extension of that scheme comprising an adaptive feedforward term whose adaptation is updated only during resets. The overall solution appears to have a peculiar nature, where the continuous-time dynamics of the FORE is augmented with the discrete-time dynamics associated with the resetting rule of [10] and with the new feedforward adaptation law proposed here.

The application that we consider is that of a turbocharged Diesel engine, which has been subject of extensive studies in the past decades. With reference to Figure 1, the Diesel engine air system is typically actuated by the use of the variable geometry turbine (VGT) guide vane position X_{VGT} and the EGR valve position X_{EGR}, in such a way that suitable operating conditions are met, as specified by operating surfaces of intermediate quantities (e.g. boost pressure and fresh air mass flow) which are usually parametrized by fuel mass flow and engine speed. A typical industrial solution encompasses a higher level controller whose multifold goals include emission regulation, which demands specific values of the intermediate quantities and consequently certain positions from the EGR and VGT actuators are requested. The actuation of the EGR valve is then performed by a lower level controller which tracks the position reference provided by the upper level controller. Accuracy and high bandwidth of the low level controller clearly helps within this nested loops control scheme, which is embedded in

*Francesco Saverio Panni and Daniel Alberer were, and Harald Waschl is with the Institute for Design and Control of Mechatronical Systems, Johannes Kepler University Linz, Altenbergerstr. 69, A-4040 Linz, Austria. (e-mail: Harald.Waschl@jku.at).

†Luca Zaccarian is with CNRS, LAAS, 7 avenue du colonel Roche, F-31400 Toulouse, France, Univ. de Toulouse, LAAS, F-31400 Toulouse, France (e-mail: zaccarian@laas.fr), and with Dipartimento di Ingegneria Industriale, University of Trento, Italy. Research supported in part by the ANR project LimICoS contract number 12 BS03 005 01, and by HYCON2 Network of Excellence "Highly-Complex and Networked Control Systems", grant agreement 257462.

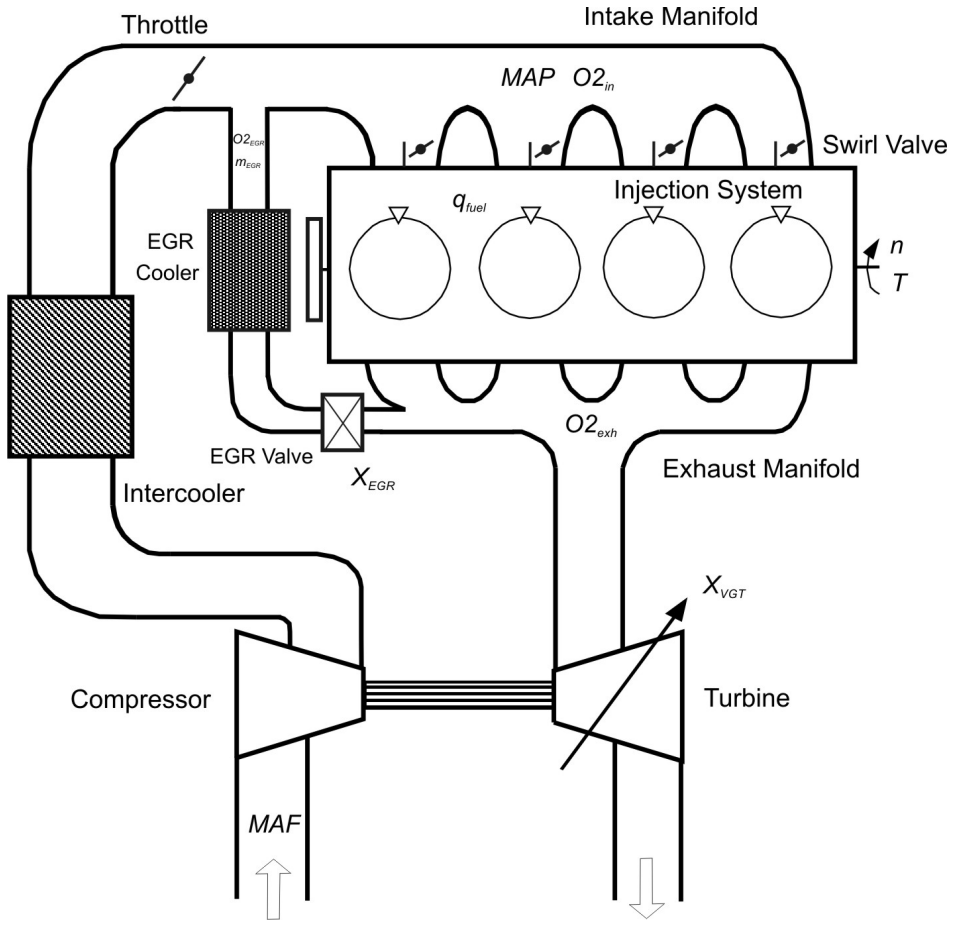

Fig. 1. The EGR valve allows part of the exhaust gas to recirculate back to the intake manifold.

the Engine Control Unit (ECU). More specifically, in the considered case of Diesel engines, EGR is mainly used to reduce nitric oxides (NO_x) emissions by replacing a part of the fresh air that is used for combustion by exhaust gases. Besides the desired reduction of NO_x, an improper use of EGR, essentially a too large amount of EGR, may lead to unacceptable high soot emissions or even to combustion instabilities. Therefore, a precise control of the EGR flow is required in particular during transient engine operations, which implies a high demand on the position control quality of the EGR valve. The use of exponentially unstable underlying continuous dynamics (induced by unstable FOREs stabilized by way of resets) is especially suited for the control of the EGR valve due to the presence of large disturbances occurring in the real application, mainly arising from the pressure difference across the valve corresponding to the pressure difference between the intake and the exhaust manifold (see Figure 1). In particular, in our application the valve is opened against the flow direction and it is experimentally acknowledged that non aggressive control actions are prone to undesired oscillations and damaging impacts of the valve on the closed position, due to the fact that transient closures of the valve cause increased pressure differences and increased disturbance magnitudes. In this sense, the aggressive controller arising from the exponentially unstable nature of the FORE solution leads to an effective closed-loop performance when implemented in the real engine, as shown in this paper. A valid alternative to our approach is that of sliding mode controllers, which have been widely used in the automotive context (see, e.g., [17], [16], [19] and references therein). The difference between the sliding mode solution and that one adopted here is that the discontinuous feedback peculiar of sliding mode typically results in an aggressive action also close to the equilibrium, whereas our technique joins a homogeneity property inducing a natural reduction of the control amplitude as the trajectory is scaled down closer to the equilibrium. Preliminary results of this work have been reported in [12] where the results of laboratory experiments are reported. Here, as compared to that work, we provide proofs of our theorems and the experimental validation on the Diesel engine testbench.

The paper is organized as follows: in Section II we discuss the proposed hybrid set-point regulation scheme and in Section III we illustrate the application of the scheme to the Diesel engine testbench. The hybrid systems notation used in the paper is the one of [5]. The reader is referred to [10, §2] for a brief overview of the corresponding mathematical framework.

II. SETPOINT REGULATION SCHEME

A. Background

According to the results in [10], set point regulation of a linear plant can be performed by way of a so-called First Order Reset Element, namely a first order linear filter with possibly unstable dynamics via a negative error feedback interconnection.

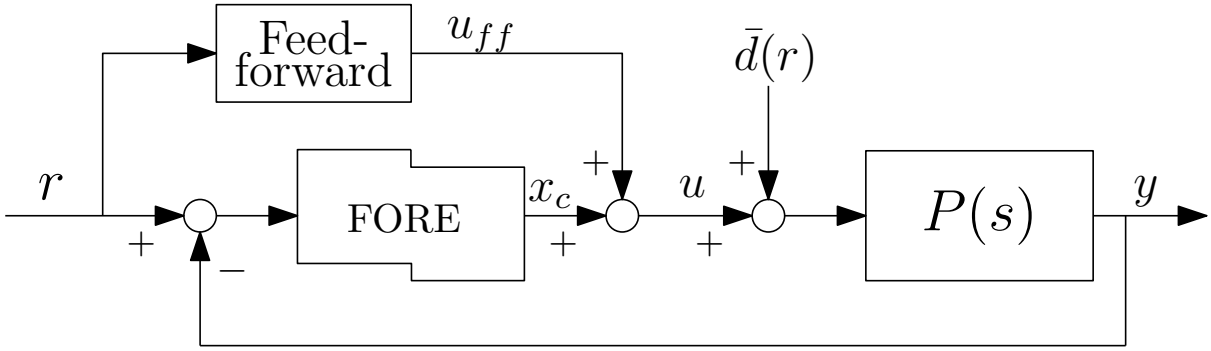

Fig. 2. FORE set-point regulator.

In particular, in [10, Theorem 1] it is established that given a constant reference r, a linear plant with transfer function $y(s) = P(s)(u(s) + \bar{d}(r))$, under the action [3] of a constant input bias $\bar{d}(r)$ (possibly depending on the reference r), a loop gain b_c and the FORE pole a_c, if wanting to perform set-point regulation of the output y to the reference r, the hybrid (or reset) controller:

$$\left.\begin{array}{l}\dot{\tau} = 1,\\ \dot{x}_c = a_c x_c + b_c v\end{array}\right\} \quad \text{if } (v, x_c, \tau) \in \mathcal{F},$$
$$\left.\begin{array}{l}\tau^+ = 0,\\ x_c^+ = 0\end{array}\right\} \quad \text{if } (v, x_c, \tau) \in \mathcal{J}, \tag{1a}$$

with

$$\begin{aligned}\mathcal{F} &= \Big\{(v, x_c, \tau),\ \text{s.t. } \varepsilon v^2 + 2 v x_c \geq 0 \text{ or } \tau \leq \rho\Big\},\\ \mathcal{J} &= \Big\{(v, x_c, \tau),\ \text{s.t. } \varepsilon v^2 + 2 v x_c \leq 0 \text{ and } \tau \geq \rho\Big\},\end{aligned} \tag{1b}$$

interconnected by $u = x_c + u_{ff}^*(r)$ with $u_{ff}^*(r) = Fr - \bar{d}(r)$, where F is the inverse of the plant static gain, guarantees asymptotic convergence of the plant output y to the reference r. The corresponding negative feedback interconnection is shown in the block diagram of Figure 2.

Remark 1: The intuition behind the scheme of Figure 2 and equation (1) is that the FORE integrates the output error, thereby enforcing an increasingly strong action on the plant (especially when $a_c > 0$) as long as the plant input is pushing in the correct direction ($x_c(r - y) \geq 0$). As soon as y reaches the set-point r, so that $x_c(r - y)$ changes sign, the FORE is reset to zero, thus being ready to possibly start integrating in the opposite direction. The feedforward term u_{ff} ensures that the FORE is only in charge of stabilizing the error dynamics. ○

Remark 2: According to the control strategy proposed in [10], the FORE dynamics in (1) is augmented with the so-called temporal regularization logic, performed by the timer variable τ. This logic is embedded in the control system to avoid Zeno phenomena and is tuned using the parameter ρ, a positive scalar (small, in general) ensuring that at least a time ρ elapses between each pair of consecutive jumps. Moreover, the resetting rule in (1) is slightly modified from the classical resetting rule first presented in [3] because of the presence of the small scalar ε, which slightly restricts the size of the jump set, thereby inducing strict decrease at jumps when dealing with planar reset systems (see [10, § III]). ○

The main drawback of this regulation scheme is that it requires knowledge of the steady-state input value $Fr - \bar{d}(r)$, namely exact knowledge of the input bias and of the plant static gain. This aspect makes it less appealing than standard PI techniques whose asymptotic tracking features result from the internal model property given by the integral action. Nevertheless, it is a fact that the transient responses achievable using a FORE are expected to be more desirable than those obtained by linear feedback. The main reason for this resides in the capability of reducing (or even eliminating) the overshoots with FOREs (see [1]) and to produce exponentially diverging transients which are then stabilized by the resets, whenever the baseline linear closed-loop before resets is exponentially unstable (see [10]).

In this paper the control scheme (1) is augmented by upgrading the feedforward action u_{ff} to become a state of the controller, which is kept constant during flows and is updated at jumps. In particular, exploiting some peculiar feature of

[3] The results in [10, Theorem 1] did not consider the constant input bias $\bar{d}(r)$ but their extension to this case is straightforward.

the FORE closed-loop which can be established in the case with scalar plants, it is shown that the state of the FORE at the reset times provides information about the required feedforward signal. The proof of exponential stability of the error dynamics will be carried out using the hybrid Lyapunov techniques of [5] (and references therein) and thereby provides the intrinsic and desirable robustness features arising from that framework.

B. A useful lemma with scalar plants

When the plant to be controlled is scalar, namely its dynamics is given by a first order linear filter, it is possible to exploit the fact that after each reset the closed-loop error dynamics starts from zero initial conditions, because the plant output error is crossing zero and the controller state is reset to zero. A technical result in this direction is provided in this section.

Consider the following first-order linear plant:

$$\dot{y} \quad = \quad a_p y + b_p(u + \bar{d}(r)) \tag{2}$$

where a_p is the plant pole and b_p is the plant input gain. Focusing on the plant (2), an online adaptation law for the feedforward signal u_{ff} is proposed, which is constant during flows and is adapted by suitable jumps at resets. Due to this special nature of the adaptation law, the following assumption is required.

Assumption 1: The origin of the reset closed-loop (2), (1) with $v = -y$, $u = x_c$ and $\bar{d}(r) = 0$ is exponentially stable. Moreover, the reset closed-loop is such that from any nonzero initial condition, there exists a finite time when the response will present a reset.

Remark 3: Note that necessary and sufficient conditions for exponential (and asymptotic) stability of the planar reset closed-loop in Assumption 1 have been given in [10, Theorem 3] and those results also allow to induce exponential stability by choosing a_c and/or b_c sufficiently large in (1). As for the other requirement in Assumption 1, it is automatically satisfied whenever the underlying linear dynamics of the closed-loop before resets generates diverging trajectories. Indeed, in that case if no resets occur, trajectories would diverge, thereby contradicting the exponential stability assumption. This is once again obtained by selecting a_c large enough in (1) and is a typical situation in practical cases where a reset controller is used. Indeed, to induce fast transients, the underlying linear dynamics is destabilized, and then resets are exploited for stabilization purposes. An example of such a design scheme is given next in Section III. ◦

Under Assumption 1 it is possible to prove the following technical lemma.

Lemma 1: Consider the closed-loop between plant (2) and controller (1) via the interconnection

$$v = r - y, \quad u = x_c + u_{ff}, \tag{3}$$

for constant values of r, $\bar{d}(r)$ and u_{ff}. Define $u^*_{ff}(r) = Fr - \bar{d}(r)$ as the steady-state control input required by the set-point regulation scheme and consider the system starting from the initial conditions $(y(0,0), x_c(0,0), \tau(0,0)) = (r, 0, 0)$.

There exists a time T, a value ρ^* and a positive scalar M_x such that for any $u_{ff} \neq u^*_{ff}(r)$ and $\rho < \rho^*$, a reset will occur at the hybrid time $(T, 0)$ and the following holds:

$$x_c(T, 0) = -M_x(u_{ff} - u^*_{ff}(r)). \tag{4}$$

Proof: For notational simplicity, define $\tilde{u}_{ff} := u_{ff} - u^*_{ff}(r)$ and, without loss of generality let us address the case $\tilde{u}_{ff} > 0$ (the opposite case can be proven following similar steps).

Consider the change of coordinates $(x_c, \tilde{y}) = (x_c, y - r)$ and notice that the closed-loop system can be written in the new coordinates as

$$\begin{bmatrix} \dot{\tilde{y}} \\ \dot{x}_c \end{bmatrix} \quad = \quad \begin{bmatrix} a_p & b_p \\ -b_c & a_c \end{bmatrix} \begin{bmatrix} \tilde{y} \\ x_c \end{bmatrix} + \begin{bmatrix} b_p \\ 0 \end{bmatrix} \tilde{u}_{ff} \tag{5a}$$

$$=: \quad A_{cl} \begin{bmatrix} \tilde{y} \\ x_c \end{bmatrix} + B_{cl}\tilde{u}_{ff}. \tag{5b}$$

Since $\tau(0,0) = 0$, then the system necessarily flows at the initial time. Moreover, due to the peculiar initial conditions $(\tilde{y}(0,0), x_c(0,0)) = (0,0)$, the upper equation in (5a) provides $\dot{\tilde{y}}(0,0) = b_p\tilde{u}_{ff} > 0$, therefore there exists T such that $y(t,0) > 0$ for all $t \in (0,T)$. Moreover, since $\dot{x}_c = -b_c\tilde{y} + a_c x_c$ and $x_c(0,0) = 0$, then $x_c(t,0) < 0$ for all $t \in (0,T)$. Select T as the maximal time with the above property and note that, by Assumption 1, T is finite because a reset must occur from any initial condition. Since during flows the dynamics of the closed-loop is linear, we can write

$$\begin{aligned} \tilde{y}(T,0) &= \begin{bmatrix} 1 & 0 \end{bmatrix} \left(\int_0^T \exp(A_{cl}(T-\tau))d\tau \right) B_{cl}\tilde{u}_{ff} = 0, \\ x_c(T,0) &= \begin{bmatrix} 0 & 1 \end{bmatrix} \left(\int_0^T \exp(A_{cl}(T-\tau))d\tau \right) B_{cl}\tilde{u}_{ff} \\ &=: -M_x\tilde{u}_{ff}, \end{aligned}$$

where necessarily $M_x > 0$, because $x_c(T,0) < 0$ and $\tilde{u}_{ff} > 0$.

From the above equations, it is evident that T is independent of $\tilde{u}_{ff}$. Moreover, as long as $\rho < \rho^* := T$, a reset will necessarily occur at time $(T,0)$, otherwise, for any $\delta > 0$, the solution at time $(T+\delta, 0)$ would flow and simultaneously satisfy $\tau > \rho$ and $\tilde{y}x_c \geq 0$, namely it would not belong to the flow set. ■

Lemma 1 is a key result to prove the effectiveness of the adaptive solution proposed in the next section. In particular, the peculiar feature that is exploited next is the fact that before any reset, the controller state is a linear function of the difference $\tilde{u}_{ff} > 0$ between the current feedforward term and the ideal (unknown) feedforward term $u^*_{ff}(r) = Fr - \bar{d}(r)$ inducing perfect tracking.

Remark 4: Assumption 1 and the strong requirement that the plant is scalar are two key properties to be able to prove the monotonicity in (4). Indeed, if Assumption 1 does not hold, then there can be defective cases where the error dynamics in (5) converges to a nonzero value of $\tilde{y}$ without any reset (even though an $\mathcal{L}_\infty$ bound on the response will hold because of exponential stability and the ISS properties established in [10, Theorem 7]). An example showing the relevance of Assumption 1 is obtained with the parameters $A_{cl} = \begin{bmatrix} a_p & b_p \\ -b_c & a_c \end{bmatrix} = \begin{bmatrix} -3 & 1 \\ -1 & -1 \end{bmatrix}$, which lead to an exponentially converging response that never resets (it can be checked, for example, running a simulation with $\bar{d} = 0$, $(y(0,0), x_c(0,0)) = 0$ and some nonzero constant reference r.

Also the requirement that the plant is a scalar filter is necessary, in general, to prove the monotonic relation (4). For example, using $a_c = 3$, $b_c = 1$ and an exponentially stable plant with two poles in $\{-1,-2\}$ and no zeros generates a response where the sign of y (therefore, also that of x_c) switches between positive and negative and vice-versa for each consecutive pairs of resets. Therefore, the state $x_c(t,j)$ before a reset does not anymore carry the information on the sign of the feedforward mismatch $\tilde{u}_{ff} > 0$, and more sophisticated proof techniques, should be adopted or more sophisticated adaptation laws should be used. A similar undesirable result is also obtained for a relative degree one stable minimum phase plant having a zero in -80 and poles in $\{-3,-2\}$, loop gain $b_c = 1$ and FORE pole $a_c = 1$.

Practical experience suggests that even for these plants the adaptation law of the next section successfully converges to the correct feedforward term, however the convergence is characterized by a peculiar oscillatory behavior of the feedforward mismatch $\tilde{u}_{ff} > 0$, which suggests that a Lyapunov proof of its convergence cannot be obtained using the convenient path involving Lemma 1. ○

C. Parametric and adaptive feedforward term

In this section we rely on the result in Lemma 1 to prove the effectiveness of a set-point regulation scheme which is based on an adaptive version of the feedforward term in Figure 2. In particular, we use the following parametric equation for u_{ff}:

$$u_{ff} = \sum_{i=1}^{N} \alpha_i \psi_i(r) = \Psi^T(r)\alpha. \tag{6}$$

In (6), the vector $\Psi(r) \in \mathbb{R}^N$ gathers together N constant independent basis functions $\psi_i(r)$ and $\alpha = \begin{bmatrix} \alpha_1 & \cdots & \alpha_N \end{bmatrix}^T$ contains the parameters to be adapted. These parameters obey the following hybrid dynamics:

$$\begin{aligned} \dot{\alpha} &= 0 && \text{if } (v, x_c, \tau) \in \mathcal{F}, \\ \alpha^+ &= \alpha + \lambda \frac{\Psi(r)}{\Psi^T(r)\Psi(r)} x_c && \text{if } (v, x_c, \tau) \in \mathcal{J}, \end{aligned} \tag{7}$$

with the flow and jump sets $\mathcal{F}$ and $\mathcal{J}$ in (1b) and where the scalar $\lambda > 0$ is a design parameter whose selection is clarified in the next proposition and in Remark 5 below. Then the following can be proven.

Proposition 1: Consider a scalar plant (2) in feedback interconnection (3) with the adaptive reset controller (1), (6), (7). Under Assumption 1 there exists a small enough ρ^* and a small enough λ^* such that for all $\rho < \rho^*$, all $\lambda < \lambda^*$, and any constant pair $(r, \bar{d}(r))$, defining the desired steady-state plant input $u^*_{ff}(r)$ as in the statement of Lemma 1, u_{ff} exponentially converges to $u^*_{ff}(r)$ and the plant output y exponentially converges to r.

Proof: First note that with the law in (7) one has:

$$\begin{aligned} u^+_{ff} &= \Psi^T(r)\alpha^+ = \Psi^T(r)\alpha + \Psi^T(r)\lambda \frac{\Psi(r)}{\Psi^T(r)\Psi(r)} x_c \\ &= u_{ff} + \lambda x_c. \end{aligned} \tag{8}$$

Then, similar to the proof of Lemma 1, consider the system in the transformed coordinates $(\tilde{y}, x_c, \tilde{u}_{ff}) = (r - y, x_c, u_{ff} - u^*_{ff}(r))$, with $u^*_{ff}(r) = Fr - \bar{d}(r)$ as in the statement of Lemma 1. Denote $x := (\tilde{y}, x_c)$. Due to Assumption 1, and from the ISS property established in [10, Theorem 7], after an initial transient, a reset will occur and we can analyze the system response starting from the initial conditions $(\tilde{y}(0,0), x_c(0,0)) = (0,0)$. Then, using the time T established in Lemma 1, we have $\tau(t,j) \in [0,T]$ for all $(t,j) \in \mathrm{dom}(\tau)$ as long as $\rho < \rho^* = T$.

Following a similar approach to the one in the proof of [10, Theorem 7], the homogeneity of the system before temporal regularization [4] and the exponential stability of Assumption 1 allow us to apply the converse Lyapunov results of [15, Theorem 2] to obtain a function $V(\tau,x)$ and positive scalars k_1, k_2, k_3, k_4, k_5 such that for all $\tilde{u}_{ff}$,

$$k_1|x|^2 \le V(\tau,x) \le k_2|x|^2, \tag{9a}$$

$$\begin{aligned}\frac{\partial V(\tau,x)}{\partial \tau} + \frac{\partial V(\tau,x)}{\partial x}\left(A_{cl}x + B_{cl}\tilde{u}_{ff}\right) \\ \le -k_3|x|^2 + k_4|x||\tilde{u}_{ff}|, \text{ if } (x,\tau)\in\mathcal{F}\end{aligned} \tag{9b}$$

$$V(0,x^+) - V(\tau,x) \le -k_5|x|^2, \text{ if } (x,\tau)\in\mathcal{J} \tag{9c}$$

Consider now the candidate Lyapunov function

$$W(\tau,x,\tilde{u}_{ff}) := V(\tau,x) + \beta|\tilde{u}_{ff}|^2 \mathrm{e}^{-\sigma\tau}, \tag{10}$$

where β and σ are positive scalars to be selected later. Since we established that $0 \le \tau(t,j) \le T$ for all $(t,j)\in \mathrm{dom}(\tau)$, this function clearly satisfies for all x, τ and $\tilde{u}_{ff}$,

$$\tilde{k}_1 \left|\begin{bmatrix} x \\ \tilde{u}_{ff}\end{bmatrix}\right|^2 \le W(\tau,x,\tilde{u}_{ff}) \le \tilde{k}_2 \left|\begin{bmatrix} x \\ \tilde{u}_{ff}\end{bmatrix}\right|^2 \tag{11}$$

with $\tilde{k}_1 := \min\{k_1, \beta \mathrm{e}^{-\sigma T}\}$ and $\tilde{k}_2 := \max\{k_2,\beta\}$. Then, using (9b), (10), and $\dot{\tilde{u}}_{ff}=0$, we get for all $\tilde{u}_{ff}$

$$\begin{aligned}\dot{W} &= \frac{\partial W(\tau,x)}{\partial \tau} + \frac{\partial W(\tau,x)}{\partial x}\left(A_{cl}x + B_{cl}\tilde{u}_{ff}\right) + \frac{\partial W(\tau,x)}{\partial \tilde{u}_{ff}} \\ &\le -k_3|x|^2 + k_4|x||\tilde{u}_{ff}| - \sigma\beta|\tilde{u}_{ff}|^2\mathrm{e}^{-\sigma T} \\ &\le -\frac{k_3}{2}|x|^2 - k_6|\tilde{u}_{ff}|^2, \qquad\qquad \text{if } (x,\tau)\in\mathcal{F},\end{aligned}$$

where we used $\tau(t,j)\le T$ and we completed squares in the last step choosing $\beta \ge \frac{\mathrm{e}^{\sigma T}}{\sigma}\left(k_6 + \frac{k_4^2}{k_3}\right)$ for any arbitrary positive scalar $k_6>0$.

Consider now the update law for u_{ff} in (8) and notice that, by virtue of (4), at jumps we have

$$\begin{aligned}\tilde{u}_{ff}^+ &= \tilde{u}_{ff} - \lambda M_x \tilde{u}_{ff} \\ &= (1-\lambda M_x)\tilde{u}_{ff} =: \mu \tilde{u}_{ff},\end{aligned} \tag{12}$$

where $|\mu|<1$ as long as $\lambda < \lambda^* := \frac{2}{M_x}$. From the above inequality, we can characterize the change of W at jumps using (9c) and (10) as follows:

$$\begin{aligned}\Delta W &:= W(0,0,\tilde{u}_{ff}^+) - W(\tilde{y},x_c,\tilde{u}_{ff}) \\ &= V(0,x^+) + \beta|\tilde{u}_{ff}^+|^2 - V(\tau,x) - \beta|\tilde{u}_{ff}|^2\mathrm{e}^{-\sigma\tau} \\ &\le -k_5|x|^2 + \beta\left(|\tilde{u}_{ff}^+|^2 - |\tilde{u}_{ff}|^2\mathrm{e}^{-\sigma T}\right) \\ &= -k_5|x|^2 + \beta(\mu^2 - \mathrm{e}^{-\sigma T})|\tilde{u}_{ff}|^2 \\ &= -k_5|x|^2 - \beta k_7|\tilde{u}_{ff}|^2, \text{ if } (x,\tau,\tilde{u}_{ff})\in\mathcal{J}\times\mathbb{R},\end{aligned}$$

where $k_7 = \mathrm{e}^{-\sigma T} - \mu^2 > 0$ as long as $\sigma \in \left(0, -\frac{2}{T}\log(|\mu|)\right)$, which is a nonempty set because $|\mu|<1$. From the properties of the Lyapunov function W during flows and across jumps, the exponential convergence result stated in the theorem follows applying standard results on Lyapunov stability of hybrid systems (see, e.g., [5]). ■

Remark 5: The characterization of $\lambda^* = \frac{2}{M_x}$ in the proof of Proposition 1 provides useful insight for tuning the parameter λ in the adaptation law (7). In particular, a useful experimental strategy is that of increasing λ until the stability limit (typically, oscillatory behavior will be experienced for values of λ around λ^*). Then, once the critical value $\lambda^* = \frac{2}{M_x}$ has been determined, a recommended strategy is to select λ as half of that value. Indeed, from equation (12) it is evident that choosing $\lambda = \frac{\lambda^*}{2} = \frac{1}{M_x}$ results in $\mu = 0$, namely a dead beat discrete dynamics for $\tilde{u}_{ff}$. The expected outcome is that, regardless of the value of r, the steady-state value of $\tilde{u}_{ff}$ is quickly determined after the first reset. ○

To avoid undesirable transients in the presence of abrupt step changes and improve performance, one may inhibit the adaptation of α in (7) when fast reference variations are detected. As customary in the adaptive control context, a possible

[4]For the sake of completeness, the converse Lyapunov results of [15, Theorem 2] require the timer τ to evolve in a compact set, so that a modified timer law should be introduced, in the same way as in [10, Theorem 7]. We omit this aspect here, to keep the discussion simple, because the result is a direct application of the technique in [10, Theorem 7].

robust implementation of this mechanism can be carried out by generating a high-pass filtered version r_f of the reference r:

$$r_f(s) = \frac{s}{s+\lambda_h} r(s) \tag{13a}$$

and then pushing to zero the adaptation gain λ if the norm of r_f is larger than a threshold $\bar{r}_f$, replacing (7) by:

$$\begin{array}{rcll} \dot{\alpha} & = & 0 & \text{if } (v, x_c, \tau) \in \mathcal{F}, \\ \alpha^+ & = & \alpha + \lambda \max\{0, \min\{1, & \text{if } (v, x_c, \tau) \in \mathcal{J}, \\ & & |\bar{r}_f - r_f|\}\} \dfrac{\Psi(r)}{\Psi^T(r)\Psi(r)} x_c & \end{array} \tag{13b}$$

Clearly, with the mechanism above, the adaptation will be only enabled as long as the piecewise constant reference dwells on each constant value for a long enough time. Moreover, this mechanism works also whenever the reference signal r is affected by noise (possibly because it comes from a higher level control system) as long as the threshold $\bar{r}_f$ is not too small.

III. Experiments on the Diesel engine testbench

The control technique proposed in Section II has been implemented on the position control of the EGR valve of a 2 liter 4 cylinder passenger car turbocharged Diesel engine, which is designed to meet the EU5 emission legislation. The engine features a common rail injection system, a variable geometry turbine turbocharger with charge air cooling and cooled high pressure exhaust gas recirculation (in accordance to the scheme of Figure 1). The engine is equipped with production standard sensors and it was operated on a highly dynamical engine test bed at the Johannes Kepler University (JKU) in Linz, represented in Figure 3. The development engine control unit (ECU) was connected to a real-time hardware-in-the-loop system for data acquisition and control. All the experiments were carried out by the use of a dSpace rapid prototyping system to control the EGR valve positioning, whereas the remaining functions of the engine control unit were kept at production standard.

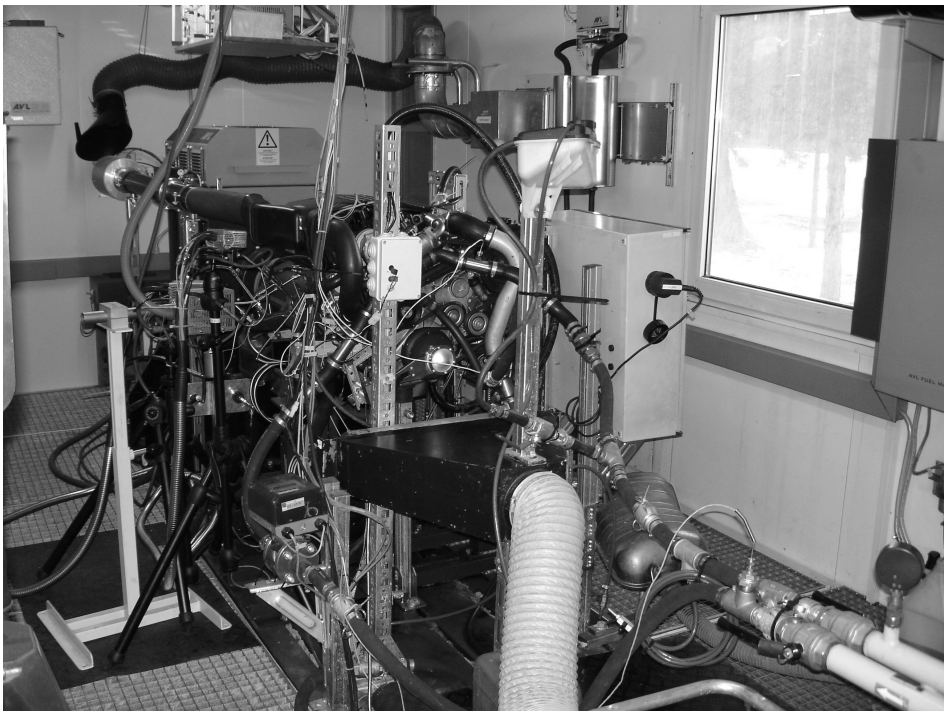

Fig. 3. The engine test bed of the Johannes Kepler University, Linz.

A. EGR valve description and regulation scheme

The EGR valve comprises a mechanical assembly which contains the valve itself and the electric brushless DC motor that drives the valve. The DC motor is a torque motor characterized by a maximum rotation of 75 degrees, a maximum torque of 540 mNm and a response time smaller than 50 ms. An embedded sensor provides a voltage output proportional to the linear position of the valve while an input voltage is used to provide the power signal to the DC motor.

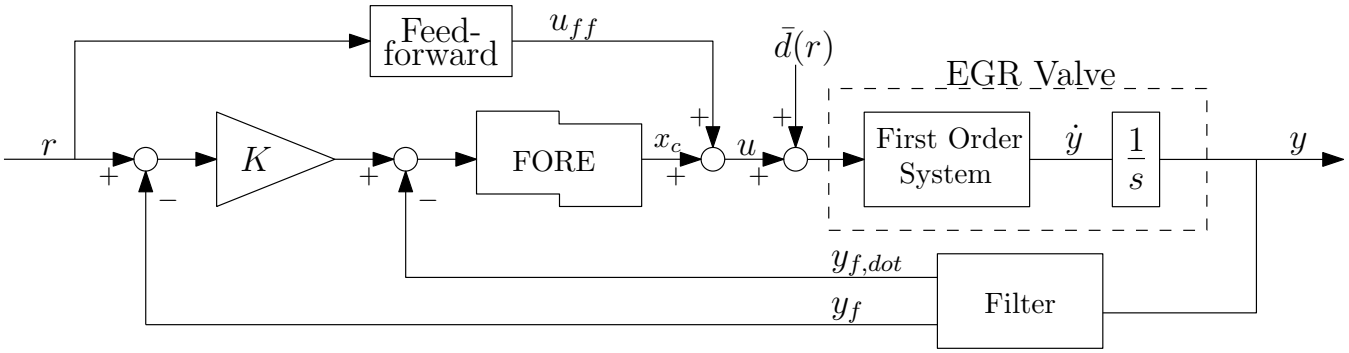

Fig. 4. Block diagram of the double-loop control scheme.

From a physical point of view, the valve can be well represented as a second order linear system with relative degree two. Indeed, neglecting the electrical time constant of the valve, the system is well represented by a second order mass-spring-damper system. Due to this fact, we apply the control strategy of Section II as the double loop scheme shown in Figure 4 where a linear dynamical filter is connected to the EGR position output to provide an estimate $\dot{y}_f$ of the EGR valve speed according to the results in [11] (alternative observer designs for plants with unknown inputs could also be employed) thereby connecting the FORE to a relative degree one system. Then the dominant dynamics from u to $\dot{y}$ is first order and, as shown in the block diagram, the FORE control system with feedforward parametrization (3), (1), (6), (7), (13) has been used in the inner loop in feedback from the estimate $\dot{y}_f$ of $\dot{y}$. The scheme in feedback from $\dot{y}_f$ is a sufficiently accurate approximation of the scheme in feedback from $\dot{y}$ as long as the filter parameters are fast enough. Finally, an outer loop regulates the position by way of the static gain K.

According to the results in [11], the filter in Figure 4 corresponds to the following high-gain observer dynamics:

$$\begin{aligned} \dot{y}_f &= y_{f,dot} + \frac{1}{\epsilon} h_p (y - y_f) \\ \dot{y}_{f,dot} &= \frac{1}{\epsilon^2} h_v (y - y_f) \end{aligned} \tag{14}$$

which provides an output y_f corresponding to a filtered version of the valve position y and an output $y_{f,dot}$ corresponding to a filtered version of its time derivative $\dot{y}$ (see [11] for details). The filter parameters are chosen as $(h_p, h_v) = (5.0,\ 6.0)$ so that the roots of the characteristic polynomial $p(\lambda) = \lambda^2 + \lambda h_p + h_v$ have negative real part. The parameter ϵ is a tuning knob: large values of ϵ correspond to a very slow filter and small values of ϵ correspond to a fast filter. The main advantage of this filter is that the tuning is easily carried out by adjusting the scalar ϵ performing a suitable trade-off between speed of the filter (smaller ϵ) and sensitivity to noise (larger ϵ). The value selected for our experiments is $\epsilon = 0.005$.

Laboratory experiments have been carried out on the valve disconnected from the motor and using a a dSpace real-time rapid prototyping system. Those experiments were used to tune the FORE parameters a_c, b_c and K and are not reported here due to space constraints but they can be found in our preliminary work [12]. According to [10], a large enough loop gain b_c and/or a large enough FORE pole a_c suffice to induce closed-loop exponential stability. Here, due to the significant stiction observed during experiments, a large value of a_c has been preferred because it leads to an aggressive action. Moreover, we expect very fast transients comprising exponentially unstable branches stabilized by resets so that Assumption 1 is satisfied too. Note that even though the theory in [10] states that arbitrarily large a_c and b_c can be employed, the effect of the sample-and-hold devices, delays in the control loop, the quantization due to the A/D and D/A converters and the presence of the filter (14) impose a limit on the parameters. In light of the above considerations, the parameters have been chosen as $a_c = 60$, $b_c = 0.013$, and $K = 140$ to induce a fast stabilization with little overshoot. Regarding the selection of λ, according to the tuning technique proposed in Remark 5, λ was increased up to the value where oscillations of u_{ff} could be observed (this corresponds to $\lambda^* = 0.64$). Then the dead-beat value was selected as half of λ^*, that is $\lambda = 0.32$. Laboratory experiments with several values of λ can be found in [12].

To suitably design the parametrization (6) we observed via experiments that the main disturbance acting on the valve is caused by the flux of the exhaust gas which pushes the EGR valve in the closing direction. This, in turns, is a static function of the pressure difference $\Delta p = p_i - p_e$ between the intake manifold pressure p_i and the exhaust manifold pressure p_e. Experimentally, it was observed that the dependence of u_{ff} on Δp is essentially affine while its dependence on r is quadratic. Therefore, we selected the parametrization in (6) as $\Psi(r, \Delta p) = [2.5\ r/100\ r^2/5000\ \Delta p/500]$, so that $\alpha \in \mathbb{R}^4$. With this selection, the feedforward action (6) comprises a bias, a linear term in Δp and a linear and a quadratic term in r. The selection above for Ψ ensures that the entries of Ψ all have the same order of magnitude during average operations, except for a larger value of the first bias term (namely the constant term of the polynomial function $u_{ff} = \Psi(r, \Delta p)^T \alpha$). This ensures that when the engine operates close to the zero valve position, where our approximation is inaccurate, the

states $\alpha_2,\ \alpha_3,\ \alpha_4$ do not deviate too much from the values providing good performance in mid-range operating conditions. Finally, the parameters of the adaptation inhibition mechanism in (13) have been tuned to $\lambda_h = 100$ and $\bar{r}_f = 50$ in such a way to avoid undesired transients in the trace of u_{ff} upon sudden changes of the reference r

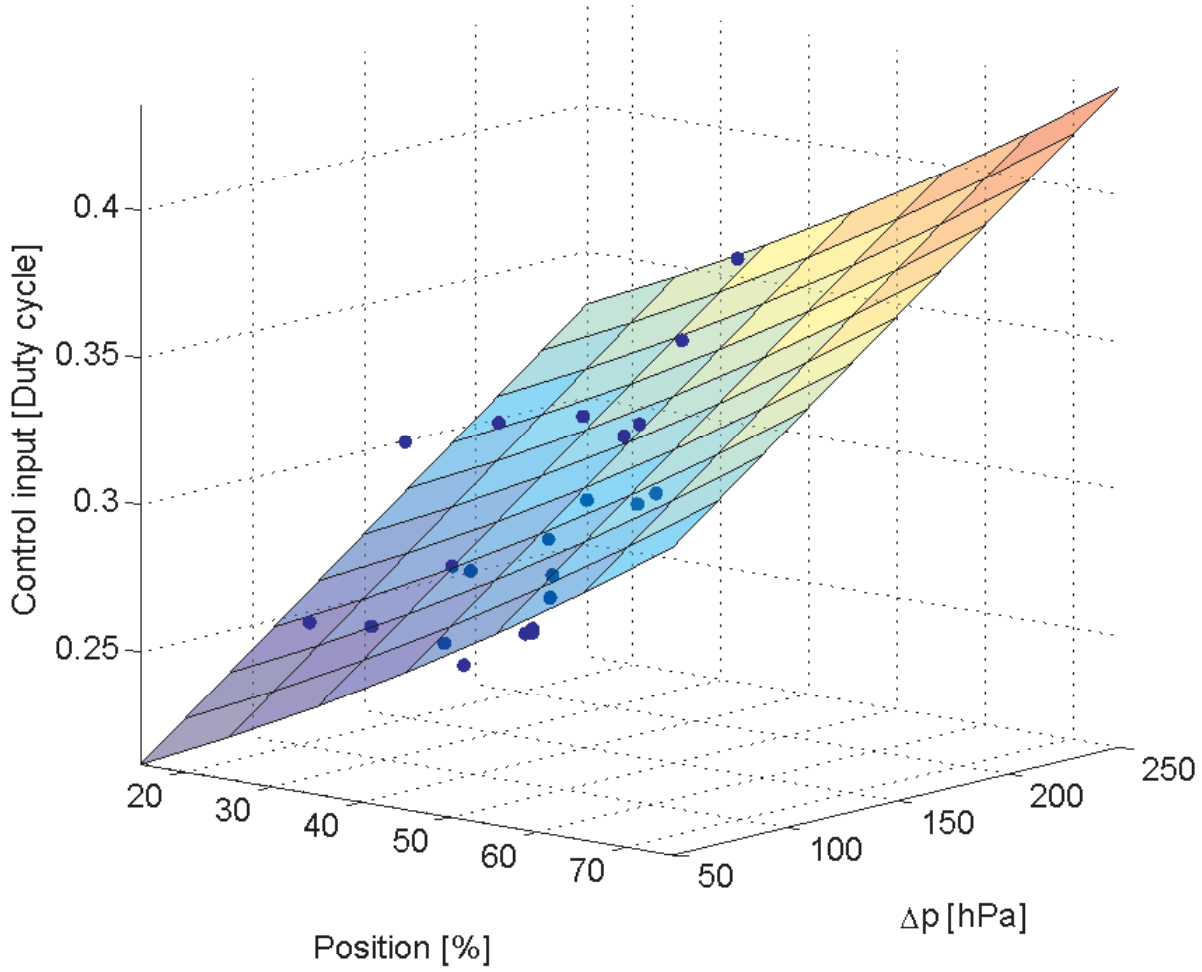

Fig. 5. Steady-state map $\Psi(r, \Delta p)^T \alpha$ after the experimental adaptation. The blue dots correspond to the measured steady-state input/output values during the experiment.

Figure 5 shows the feedforward surface $\Psi(r, \Delta p)^T \alpha$ after an experimental adaptation of α with changing engine conditions. The blue dots represent the steady-state input-output pairs observed during the experimental run.

Remark 6: Since in the Diesel engine application the FORE control system is subject to temporary disturbances mostly arising from the closed-loop effects of the VGT, practical experience revealed that it is advantageous to saturate the update term $\frac{\Psi}{\Psi^T\Psi} x_c$ in (13b) so that excessively large updates of α due to transient disturbances do not occur. For our application we used $\frac{\Psi}{\Psi^T\Psi} \sigma_{0.3}(x_c)$, where $\sigma_M(s) = \text{sign}(s) \min\{|s|, M\}$ is the standard scalar saturation function. Note that this does not correspond to limiting u in that set due to the presence of u_{ff} in the second equation of (3). An alternative to this is to design a more conservative controller by reducing the FORE parameters. However, using saturation gives the advantage of not affecting the aggressive small signal behavior and only toning down the large signal responses. ○

B. Experimental results

To carry out comparative experiments on the engine testbench, the bypass feature available for certain ECU signals has been used. This allowed us to leave unchanged the higher level controller, while the production standard EGR valve position controller coded in the ECU (this is a gain scheduled PID controller) was replaced by the FORE controller, which was running in the dSpace hardware-software setup connected to the testbench. Moreover, the testbench allowed for the monitoring of several engine outputs whose behavior is reported in this section.

A first set of experiments was performed bypassing the EGR position reference coming from the higher level controller and requiring a step change of the EGR valve position during a steady operation phase of the engine, so as to compare the step

responses obtained by our controller and by the production standard one. Figure 6 was obtained with the engine running at speed $2200\ rpm$ ($\approx 37\ Hz$) and fuel amount of $30\ mg/cycle$. Here, the solid curve corresponds to the response of the FORE controller and should be compared to the dashed curve, obtained when delivering the step reference to the ECU production standard controller, which is based on a gain scheduled PID plus feedforward architecture. The high frequency oscillations on the measured position (upper plot) are caused by the air flow peaks through the EGR valve caused by the combustion cycles. Their frequency (roughly $75\ Hz$) is four times larger than a complete cycle of the engine (roughly $18\ Hz$ – note that each cycle requires two engine revolutions therefore this frequency is half of the engine rotation frequency). The third trace reveals also oscillations of Δp which exhibit the two above discussed fundamental frequencies of 18 and $75\ Hz$. The feedforward action $u_{ff} = \Psi(r, \Delta p)^T \alpha$ is effective at making this disturbance almost invisible on the position error, where only the residual $75\ Hz$ component is visible. The rest of the job is carried out by the exponentially diverging branches of the input u. The lower plot of Figure 6 shows the adapted parameters α. Notice that the parameters remain essentially constant because they have already converged to the steady-state values. For experiments illustrating the convergence transients of the parameters α, see the ones reported in our preliminary work [12, Figs. 4 & 7]. Note that, according to the discussion of Section III-A, the bias term α_1 exhibits more visible variations due to the choice of the normalization factors in the function $\Psi(r, \Delta p)$.

A second, perhaps more significant, test carried out on the engine testbench was to compare the EGR valve positioning accuracy when using the ECU production standard controller and the proposed FORE controller through the ECE 15 urban driving cycle, which lasts 195 seconds.

The response of the FORE is compared to the one of the production standard ECU controller in Figures 7 and 8. Such a comparison clearly infers that the FORE allows for a much faster tracking of the reference position. In particular Figure 7 and the two top plots of Figure 8 clearly reveal the higher precision of the hybrid controller. Looking at the lower plot of Figure 8 it is also possible to appreciate the impact on the NO_x emissions when using the FORE scheme. In particular, not surprisingly, the most relevant difference of the NO_x emissions is visible whenever an opening of the EGR valve is requested by the higher-level control system (see the transient response around time $t = 117$). Indeed, the reduced position tracking error given by the FORE controller ensures a prompt gas recirculation and a reduced amount of emissions. One may also expect that the large position error experienced by the ECU control system in the time interval $t \in [119, 120]$ could have an impact on the emissions but this is not the case because this error does not impact much the EGR flow. Instead in the previously commented phase, where the EGR valve is almost closed, the FORE position controller accuracy has a strong impact on the EGR flow.

To numerically quantify the gap between the two controllers, we also consider the mean squared position error achieved by the two controllers in the considered ECE 15 cycle, namely

$$MSE = \frac{1}{|\mathcal{I}|} \sum_{i \in \mathcal{I}} e_i^2, \quad \mathcal{I} = \{i \in \{1, \dots, n\} : \ r_i \neq 0\} \tag{15}$$

where e_i corresponds to the i-the sample of the difference between the position reference (dashed line in Figures 7 and 8) and the valve position (solid lines in the same figures). The sampling period of the signals is $1\ ms$ over the $195\ s$ ECE 15 urban cycle. The computed MSE correspond to 6.6794 for the ECU controller and 1.5343 for the FORE controller. The latter is 23% of the former thus revealing that the FORE scheme reduces the MSE to less than one fourth than that obtained with the production standard controller. Clearly this is a preliminary result and extensive experimental tests should be performed to obtain a thorough comparison of the two schemes in terms of performance and robustness. Nevertheless, these preliminary experimental results reveal some interesting potential behind our reset control technique.

IV. Acknowledgments

This work has been partly carried out at LCM GmbH as part of a K2 project. K2 projects are financed using funding from the Austrian COMET-K2 programme. The COMET K2 projects at LCM are supported by the Austrian federal government, the federal state of Upper Austria, the Johannes Kepler University and all the K2-COMET scientific partners.

References

[1] O. Beker, C.V. Hollot, and Y. Chait. Plant with an integrator: an example of reset control overcoming limitations of linear feedback. *IEEE Transactions Automatic Control*, 46:1797–1799, 2001.
[2] O. Beker, C.V. Hollot, Y. Chait, and H. Han. Fundamental properties of reset control systems. *Automatica*, 40:905–915, 2004.
[3] J.C. Clegg. A nonlinear integrator for servomechanisms. *Transactions of the A.I.E.E.*, 77 (Part II):41–42, 1958.
[4] J.A. Cook, J. Sun, J.H. Buckland, I.V. Kolmanovsky, H. Peng, and J.W. Grizzle. Automotive powertrain control: A survey. *Asian Journal of Control*, 8(3):237–260, 2006.
[5] R. Goebel, R. Sanfelice, and A.R. Teel. Hybrid dynamical systems. *IEEE Control Systems Magazine*, 29(2):28–93, April 2009.
[6] L. Guzzella and C.H. Onder. *Introduction to modeling and control of internal combustion engine systems*. Springer Verlag, 2010.
[7] I. Horowitz and P. Rosenbaum. Non-linear design for cost of feedback reduction in systems with large parameter uncertainty. *International Journal of Control*, 21:977–1001, 1975.
[8] M. Jankovic and I. Kolmanovsky. Constructive Lyapunov control design for turbocharged Diesel engines. *IEEE Transactions on Control Systems Technology*, 8(2):288–299, 2000.

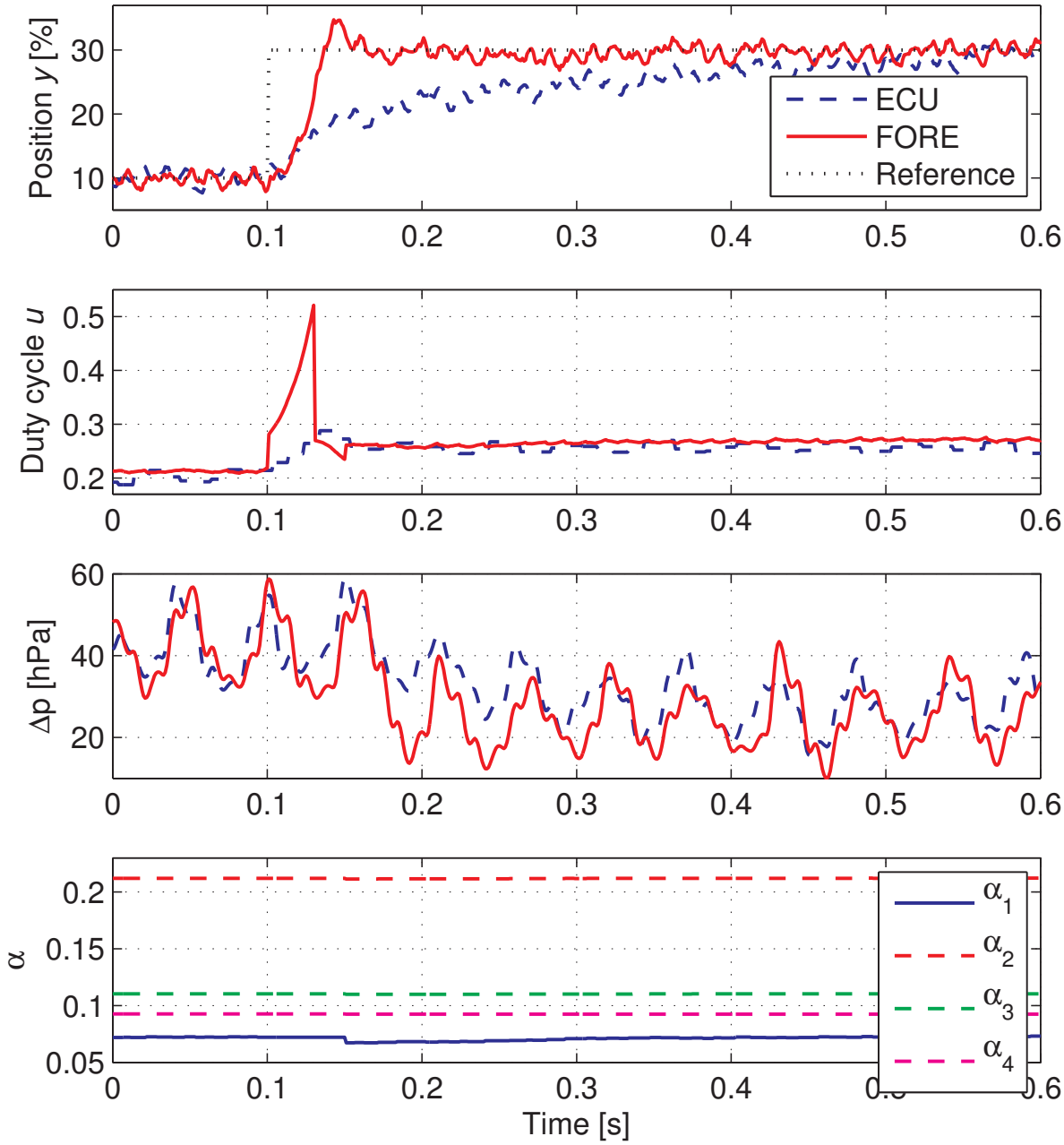

Fig. 6. Comparison of the step responses of the proposed FORE controller and of the ECU production standard controller.

[9] T.V. Johnson. Review of Diesel emissions and control. *International Journal of Engine Research*, 10(5):275–285, 2009.

[10] D. Nešić, A.R. Teel, and L. Zaccarian. Stability and performance of SISO control systems with First Order Reset Elements. *IEEE Transactions on Automatic Control*, 56(11):2567–2582, 2011.

[11] S. Nicosia, A. Tornambè, and P. Valigi. Experimental results in state estimation of industrial robots. In *IEEE Conference on Decision and Control*, pages 360–365, December 1990.

[12] F.S. Panni, D. Alberer, and L. Zaccarian. Set-point regulation of an EGR valve using a FORE with hybrid input bias estimation. In *IEEE American Control Conference*, pages 4221–4226, Montreal, Canada, June 2012.

[13] R. Sharma, D. Nesic, and C. Manzie. Model reduction of turbocharged (TC) spark ignition (SI) engines. *IEEE Transactions on control Systems Technology*, 19(2):297–310, 2011.

[14] G. Stewart and F. Borrelli. A model predictive control framework for industrial turbodiesel engine control. In *IEEE Conference on Decision and Control*, pages 5704–5711, 2008.

[15] S.E. Tuna and A.R. Teel. Homogeneous hybrid systems and a converse Lyapunov theorem. In *45th IEEE Conference on Decision and Control*, pages 6235–6240, December 2006.

[16] D. Upadhyay, V. Utkin, and G. Rizzoni. Multivariable control design for intake flow regulation of a Diesel engine using sliding mode. In *15th IFAC World Congress*, 2002.

[17] V. Utkin, H.C. Chang, I. Kolmanovsky, and J.A. Cook. Sliding mode control for variable geometry turbocharged Diesel engines. In *IEEE American Control Conference*, pages 584–588, 2000.

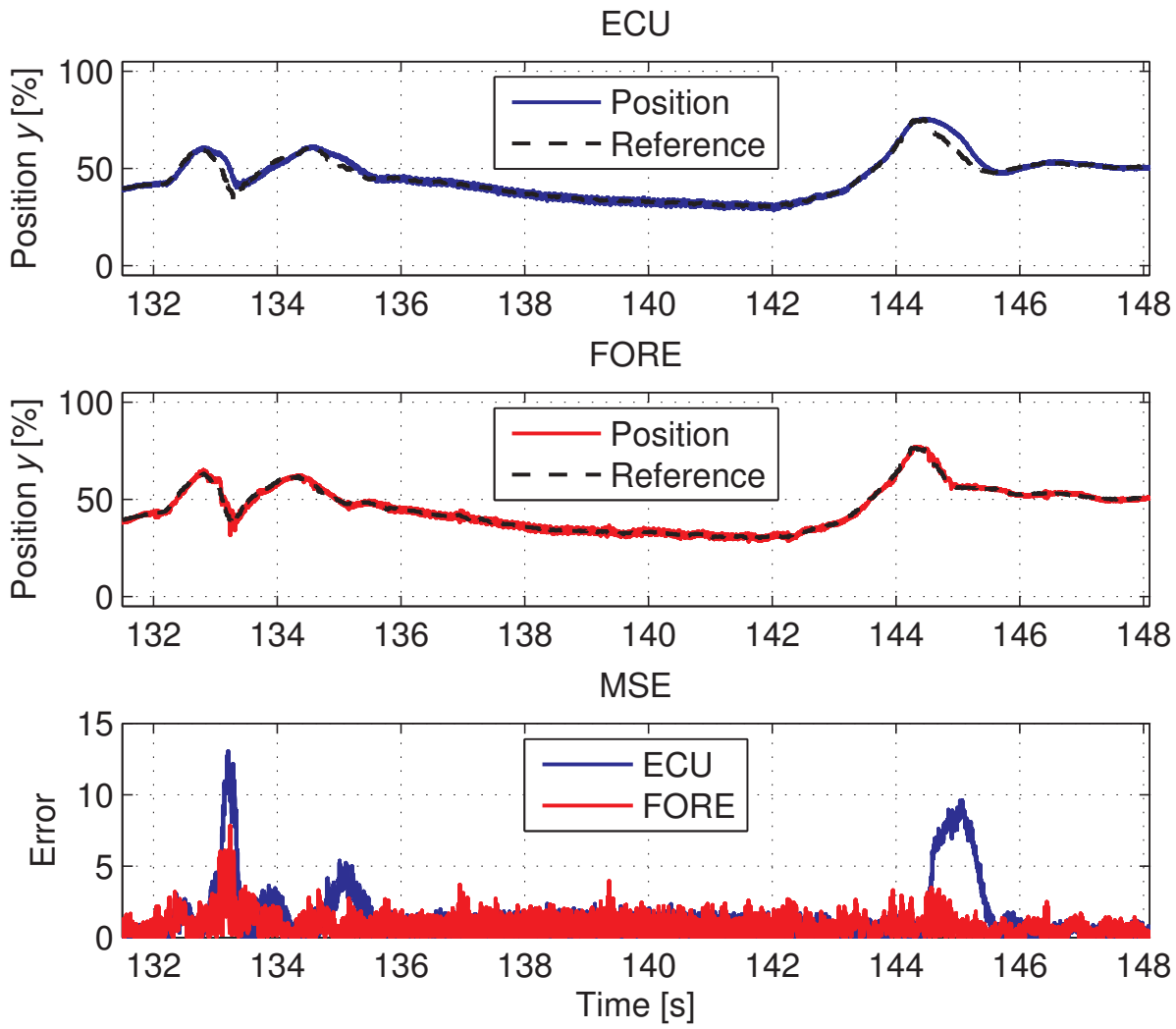

Fig. 7. ECU and FORE responses on a portion of the ECE 15 cycle.

[18] M. van Nieuwstadt, P.E. Moraal, I. Kolmanovsky, A. Stefanopoulou, P. Wood, and M. Criddle. Decentralized and multivariable designs for EGR-VGT control of a Diesel engine. In *2nd IFAC Workshop on Advances in Automotive Control*, 1998.

[19] J. Wang. Hybrid robust air-path control for Diesel engines operating conventional and low temperature combustion modes. *IEEE Transactions on Control Systems Technology*, 16(6):1138–1151, 2008.

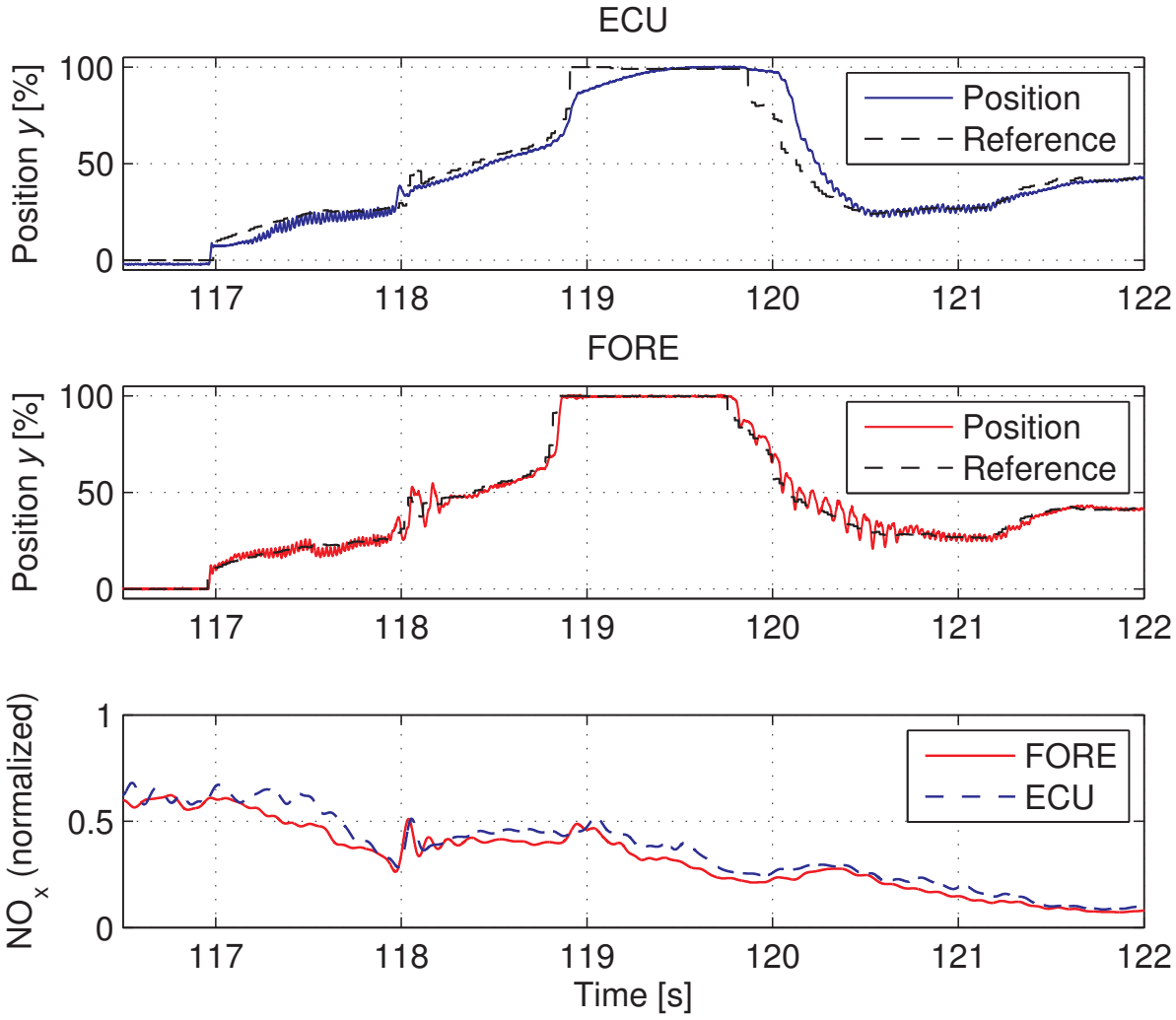

Fig. 8. ECU and FORE responses on a portion of the ECE 15 cycle together with NO_x emissions.